Materials Research Express

PAPER

A comprehensive study of $Co_{1-x}Ni_xFe_2O_4$ nanoparticles fabricated via three different synthetic methods

To cite this article: M S Pessoa *et al* 2019 *Mater. Res. Express* **6** 125068

Materials Research Express

PAPER

A comprehensive study of $Co_{1-x}Ni_xFe_2O_4$ nanoparticles fabricated via three different synthetic methods

RECEIVED
14 August 2019

REVISED
4 November 2019

ACCEPTED FOR PUBLICATION
20 November 2019

PUBLISHED
29 November 2019

M S Pessoa[1], P S Moscon[1], R S Melo[2], A Franco Jr[2] and P C Morais[3,4]

[1] Universidade Federal do Espírito Santo, Departamento de Ciências Naturais, São Mateus ES 29932-540, Brazil
[2] Universidade Federal de Goiás, Instituto de Física, Goiânia GO 74001-970, Brazil
[3] Universidade de Brasília, Instituto de Física, Brasília DF 70910-900, Brazil
[4] Universidade Católica de Brasília, Programa de Pós-Graduação em Ciências Genômicas e Biotecnologia, Brasília DF 70790-160, Brazil

E-mail: marcio.pessoa@ufes.br

Keywords: nickel-cobalt ferrite, nanoparticle, combustion, hydrothermal, hydrolysis, ferromagnetic resonance spectrum simulation, physical properties

Abstract

We report on three different synthetic methods for producing $Co_{1-x}Ni_xFe_2O_4$ nanoparticles ($x = 0.0$, 0.4, and 1.0): combustion (C), hydrothermal (HT), and forced hydrolysis (FH). Theoretical fittings of the ferromagnetic resonance (FMR) lines were achieved by considering a proposed four-fold symmetry model for randomly dispersed magnetic nanoparticles (NPs). The average grain size (D), between 10 and 80 nm, and magnetic properties are found to depend strongly on both the selectedsynthesis route and stoichiometry (x). Interestingly, while the HT- and FH-methods provide NPs with no systematic dependence of coercive field and remanence, upon x or D, the C-method showedmonotonic dependence. The magnetocrystalline anisotropy field (H_a), extracted from simulating the FMR spectra, systematically reduces with increasing x, regardless the synthetic route used. Worth mentioning that the largest (smallest) variation in H_a is observed for the C-method (HT-method) equals to $\Delta H_a = -3853$ Oe ($\Delta H_a = -1676$ Oe).

1. Introduction

Iron-based cubic ferrites (spinelstructures) are ferromagnetic materialswith general formula MFe_2O_4(M^{2+}=Fe^{2+}, Ni^{2+}, Co^{2+}, Mn^{2+}, Cu^{2+}, Zn^{2+}, Cd^{2+}, etc). Such stoichiometry results in facecentered cubic(fcc) spinel structures, with Fe^{3+} and M^{2+} occupying respectively octahedral and tetrahedral sites (called normal spinel structure) or, alternatively, half Fe^{3+} filling tetrahedral sites while the remaining ions (M^{2+} and half Fe^{3+}) occupying octahedral sites(called inverse spinel structure) [1]. Very often, cubic ferrites present a mixed structure between normal spinel and inverse spinel [2]. More recently, nanocrystalline cubic ferrites have been intensively investigated, focusing on both basic and technological aspects given their simple processing, low cost of production, easy scalability, size and shape modulation, high chemical stability, improved biocompatibility and wide range of applications in fields as diverse as drug delivery, magnetic resonance imaging (MRI), magneto hyperthermia, temperature sensor, gas sensor, data storage, catalysis, among others [3–8]. Application to a specific technology depends on the morphological, structural, magnetic and surface functionalization characteristics. These characteristics are determined by: (i) method of synthesis [9, 10]; (ii) thermal/timetreatment [11, 12]; (iii) surface functionalization [13]; and (iv) sintering atmosphere [11, 12]. In a more broad approach the M^{2+} cation may be a mixture of different ions, including only Fe^{2+} while resulting in magnetite ($Fe^{2+}Fe_2^{3+}O_4$) [14–22]. The variation in combining different M^{2+} ions, changing synthesis routes and surface modulation via different coatings allows great diversification of the characteristics of the obtained materials and, consequently, leading to appropriate characteristics for different applications. As an example it is worth mentioning the papers by Gholizadeh and Shamgani&Gholizadeh reporting significant change in the redox and catalytic properties by varying the relative ratio of metals ions in lanthanum and multi-metal ferrites [8, 22].

In this study, different synthesis techniques, namely combustion (C), forced hydrolysis (FH) and hydrothermal (HT) are used to produce nanosized iron-based mixed cubic ferrites ($Co_{1-x}Ni_xFe_2O_4$) with nominal identical stoichiometry ($x = 0.0, 0.4$, and 1.0). The study covers a gap in the literature in this regard and aims to investigate the influence of different synthetic routes employed upon the structural and magnetic characteristics of the Co, Co/Ni and Ni nanosized cubic ferrites particles. For magnetic and structural analyses, magnetization measurements, x-ray diffraction (XRD) and ferromagnetic resonance (FMR) were systematically employed. In particular, through theoretical simulations, the FMR technique allowed us to obtain componentsand values of the crystalline anisotropy. We emphasize that there are few papers in the literature applying the FMR technique for these purposes while the analysis herein introduced represents a major contribution to the field. Moreover, the present study emphasizes the key role played by changing the synthesis technique while preparing nanosized cubic ferrite particles with the same nominal stoichiometry, but with diversified physical properties.

2. Materials and methods

Three sets of nanoparticulate $Co_{1-x}Ni_xFe_2O_4$ samples ($x = 0.0, 0.4$, and 1.0) were herein prepared using (i) combustion reaction [15], (ii) forced hydrolysis [16]and (iii) hydrothermal [17] methods. All reagents were of analytical grade and were used without any further purification(Aldrich, NJ—USA). Reagents manipulations and reactions were all carried out in air under a fume-hood without inert gas purging. For sample preparation employing the C-method, cobalt nitrate ($Co(NO_3)_2.6H_2O$), nickel nitrate ($Ni(NO_3)_2.6H_2O$), iron nitrate ($Fe(NO_3)_3.9H_2O$) and urea (CH_4N_2O)were used as starting materials. Reagents were mixed to meet the desired stoichiometry ($x = 0.0, 0.4$, and 1.0) whereas urea was used as fuel and the synthesis progressed without intermediate decomposition and/or calcination steps.

For sample preparation employing the FH-method, iron nitrate ($Fe(NO_3)_3.9H_2O$), nickel nitrate ($Ni(NO_3)_2.6H_2O$) and cobalt acetate ($Co(CH_3CO_2)_2.4H_2O$) were used as starting materials. Reagents were weighted to meet the desired stoichiometry ($x = 0.0, 0.4$, and 1.0) and dispersed into 250 ml of 1,2-propanediol ($C_3H_8O_2$). The total metal concentration was 0.3 mol l^{-1} whereas the hydrolysis ratio and the acetate content were fixed at 9 and 3, respectively. For all reactions, the starting mixture containing the salts, deionized water, sodium acetate and 1,2-propanediol was heated to 160 °C with a heating rate of 10 °C min^{-1}. A black colloidal suspension was obtained after refluxing the mixture for 5 h. Next, the black suspension was kept in air at 100 °C for extra 12 h. The black precipitate was separated from the suspension by centrifugation and washed several times with water and ethanol. The resultant powders were dried in air at 50 °C.

For sample preparation employing the HT-method, 0.1 mol l^{-1} aqueous solutions of each nitrate (Co, Ni, and Fe) were prepared and mixed to meet the desired stoichiometry ($x = 0.0, 0.4$, and 1.0). The pH of each mixture was adjusted to 12 by addition (drop wise) of 2 mol l^{-1} aqueous solution of sodium hydroxide (NaOH), under moderated stirring for 30 min at room temperature. The pH-adjusted mixture was subsequently transferred to a Teflon lined stainless steel autoclave, which was placed inside a muffle furnace with temperature set at 180 °C, dwelling for 12 h. Afterwards, the autoclave was removed out of the furnace and slowly cooled down to room temperature. The resulting brownish precipitate was rinsed several times with distilled water (MILIQ water) and ethanol to remove excess of reagents and impurities. Finally, the brownish precipitate was dried in an oven at 100 °C for about 3 h.

The FMR spectra of all samples were recorded at room temperature using the EMX plus Bruker spectrometer (Bruker, Germany) equipped with an X-band (9.86 GHz) high sensitivity resonator (Bruker ER 4119HS, Germany). The instrumental settings for FMR measurements were 0.1 mW microwave power, 5 G amplitude modulation, 100 kHz modulation frequency, 14 000 G sweep width, 7,000 G central field, and 500 s sweep time. The FMR spectra analyses were carried out following the original model proposed by Tsay *et al* [23]. According to these authors, the FMR lineshape is defined by a random distribution of resonance conditions associated with the random directional distribution of the crystalline axes relative to the applied magnetic field. From the FMR lineshape analysis it is possible to estimate the magnetocrystalline anisotropy field (H_a), the *g*-factor (*g*), and the dispersion parameter (*W*). It is worth stressing that the *W* parameter does not correspond to the spectral peak-to-peak width (ΔH_{pp}); it is just a theoretical parameter that quantifies the anisotropy distribution around specific values of crystalline anisotropy, as explained in detail in the literature [24]. There are different approaches in the literature explaining the evolution of the FMR linewidth (ΔH_{pp}), as for instance in terms of the temperature [25].

For each sample, the hysteresis loops (*M* versus *H*) were recorded at room temperature using the Model EV-9Vibrating Sample Magnetometer (VSM) from ADE Magnetics. Likewise, in order to assess the structural parameters, XRD data were recorded for all synthesized samples, using a Shimadzu diffractometer (model 6000) equipped with CuKα radiation ($\lambda = 1.5418$ Å) and scanning rate set at 21 min at a fixed time of 3 s for a wide

range of Bragg angles ($10^\circ \leqslant 2\theta \leqslant 90^\circ$). Database (JCPDS) of single phased $CoFe_2O_4$ and $NiFe_2O_4$, and Rietveld refinement method, were carried out by using the software package General Structure Analysis Software-II (GSAS-II). The crystallite sizes were determined by the Scherrer equation:

$$D_{hkl} = \frac{k\lambda}{\beta(\cos\theta)}, \quad (1)$$

where k is constant depending on particle shape herein considered for spherical particles ($k \approx 0.9$), λ is the wavelength (1.5418 Å) of electromagnetic radiation, θ is diffraction angle and β is the corrected (relative to crystalline Si) width at half height of the diffraction peak (FWHM). The crystallite densities were obtained by the relation:

$$\rho = \frac{nA}{V_C N_A}, \quad (2)$$

where n is the number of atoms associated to each unit cell, A is the atomic weight, V_C is the unit cell volume determined from the Rietveld refinement, and N_A is the Avogadro's number.

3. Results and discussion

XRD patterns of all synthesized samples ($Co_{1-x}Ni_xFe_2O_4$; $x = 0.0$, 0.4, and 1.0), obtained from the three different synthesizing techniques (C, FH, and HT), are shown in figure 1. The as-synthesized samples exhibit the XRD peaks indicative of single-phased spinel crystal structure. Differently from the syntheses performed via the C-and HT-method, the synthesis performed via the FH-method leads to nanoparticulate $Co_{1-x}Ni_xFe_2O_4$ samples with lower degree of crystallinity, as indicated by the broadening of the XRD peaks shown in figure 1(c). For comparison, standard XRD patterns (JCPDS files) of both Fe_2O_4 and $NiFe_2O_4$ phases are included (see vertical black and red solid lines) in the bottom of the panel, left hand-side column (see figure 1).

The estimated lattice parameter (a), average grain size (D), unit cell volume (V) and mass density (ρ) of all synthesized samples are collectedin table 1, from which differences in average grain size as a function of the Co/Ni ratio is clearly demonstrated. For the HT-method, the average grain size increases monotonically as the nickel content increases, ranging from 16 nm up to 80 nm. Inversely, for the samples obtained usingthe C-method the average grain size reduces as the nickel content increases, ranging from 52 nm down to 33 nm; in this case for $x = 0.4$ and $x = 1.0$ no significant variation was observed. No systematic dependence of the average grain sizewith the nickel content is observed in the samples synthesized via the FH-method. However, the synthesis via the FH-method provides samples with average grain sizes below 10 nm whereas both C-and HT-method provide samples with average grain sizes above 15 nm. For comparison, the goodness-of-fit (GOF) parameter is plotted in the last row of table 1.

Room-temperature hysteresis cycles of all prepared samples ($Co_{1-x}Ni_xFe_2O_4$; $x = 0.0$, 0.4, and 1.0), obtained from the three synthesis techniques (C, FH, and HT), are shown in figure 2. Magnified curves, at lower applied fields, are shown in the insets of all panels in figure 2. At room temperature, typical ferrimagnetic behavior is observed for all samplessynthesized via the C- and HT-method, whereas all samples obtained via the FH-method present the usual superparamagnetic behavior. As shown in figure 2(c), the observed magnetic characteristics agree well with the reduced sizes extracted from the XRD measurements, as the superparamagnetic behavior is observed in samples presenting nanoparticle sizes below 10 nm, indicating that thermal fluctuation does overcome the magnetocrystalline energy and/or magnetic particle-particle coupling at room temperature. In addition to the superparamagnetic behavior, the impact of a remarkable surface-to-volume ratio in nanoparticles with sizes below 10 nm may lead to spin-glass-like behavior in the shell layer, in contrast with a more crystalline and magnetically-ordered core. These two characteristics may help understand the reduced values of the saturation magnetization obtained for the samples synthesized via the FH-method [26]. Herein, the saturation magnetizations were determined by extrapolating M versus $1/H$ to $1/H \rightarrow 0$, as described in the literature [27].

Data collected in tables 1 and 2 show that the saturation magnetization (M_s) increases with increasing average grain size for samples synthesized via both C- and FH-method, i.e. the larger the grain size the higher the saturation magnetization [26]. Slight deviation from this trend, as observed for the samples synthesized via the C-method ($x = 0.4$ and 1.0), reveals the complexity of the magnetic system in regard to two extra points. First, the higher saturation magnetization reported for cobalt-rich ferrite as opposed to lower saturation magnetization observed in nickel-rich ferrite [26]. Second, the degree of magnetic ion (Fe^{3+}, Co^{2+}, and Ni^{2+}) occupancy in the tetrahedral and octahedral sites [28]. In this particular case, as the systems have similar grain sizes (33 and 35 nm), we conclude that: (1) the degree of magnetic ions occupancy surpasses the effects of both grain size and nickel-content; and/or (2) the shell-to-core ratio is higher for the cobalt-rich sample. Finally, the samples synthesized via the HT-method show the opposite trend in regard to two aspects, namely size-

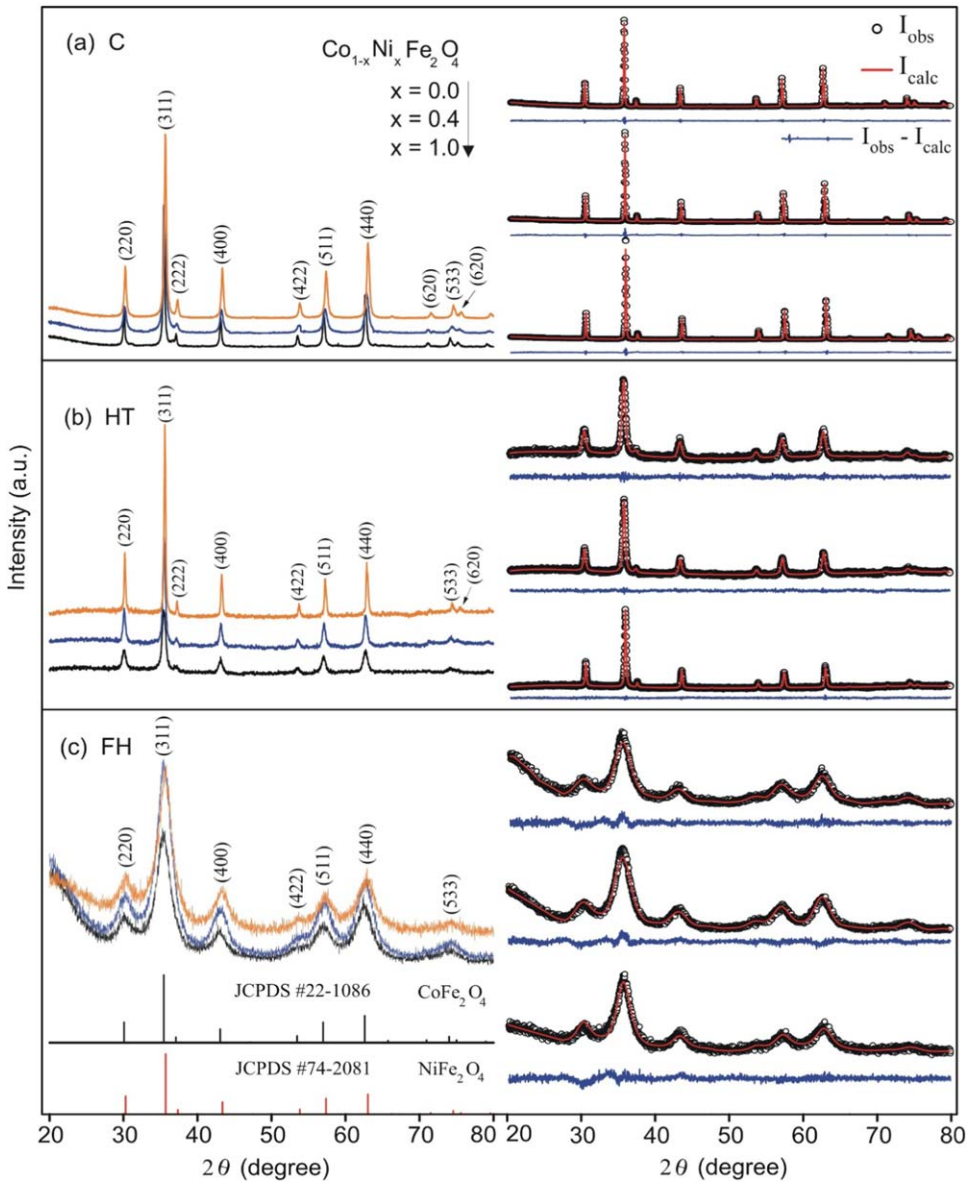

Figure 1. X-ray diffraction patterns of $Co_{1-x}Ni_xFe_2O_4$ powder obtained by (a) combustion (C), (b) hydrothermal (HT), and (c) forced hydrolysis (FH). In each horizontal panel the curves obtained for $x = 0.0$, 0.4 and 1.0 are positioned in the upper, middle and lower position, respectively, as indicated by the arrow in the upper left hand-side panel. The respective Rietveld refinements are shown, from top to bottom, in the right hand-side column.

Table 1. Parameters estimated from XRD data recorded from the $Co_{1-x}Ni_xFe_2O_4$ samples.

	C-method			HT-method			FH-method		
Parameters	$x = 0.0$	$x = 0.4$	$x = 1.0$	$x = 0.0$	$x = 0.4$	$x = 1.0$	$x = 0.0$	$x = 0.4$	$x = 1.0$
a (Å)	8.376	8.419	8.335	8.379	8.368	8.346	8.394	8.394	8.401
D(nm)	52	35	33	16	36	80	8.9	9.3	5.5
V(Å^3)	587.7	596.7	579.1	588.3	586.0	581.4	591.4	594.4	592.9
ρ (g cm^{-3})	5.304	5.154	5.344	5.299	5.319	5.323	5.270	5.270	5.220
GOF	1.69	4.38	2.47	0.67	0.77	0.78	1.16	1.26	2.01

dependence and nickel-content. Likely, the magnetic ion (Fe^{3+}, Co^{2+}, and Ni^{2+}) site occupancy is strongly influenced while using the HT-method to synthesize mixed cobalt-nickel cubic ferrites ($Co_{1-x}Ni_xFe_2O_4$). Therefore, except for the synthesis route using the HT-method, our findings regarding both C- and FH-method suggest that grain size and cation distribution are the main mechanisms for determining saturation magnetization in mixed cobalt-nickel cubic ferrites.

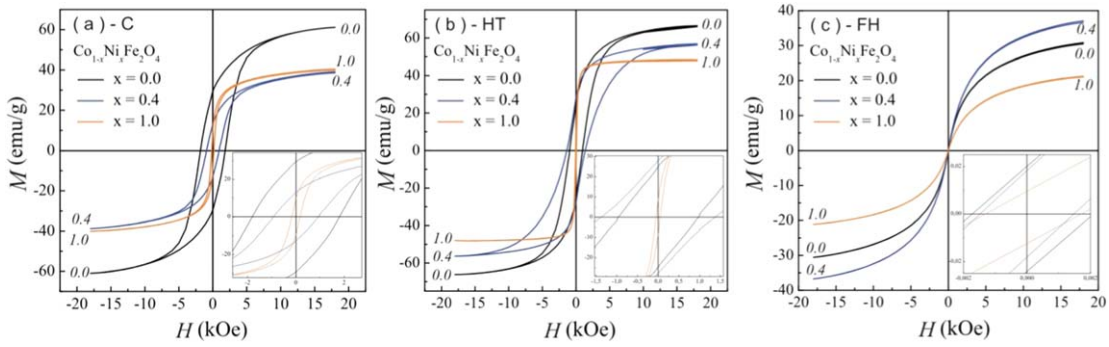

Figure 2. Hysteresis loops for the $Co_{1-x}Ni_xFe_2O_4$ samples synthesized via (a) combustion (C), (b) hydrothermal (HT), and (c) forced hydrolysis (FH). Nickel-contents $x = 0.0$, 0.4 and 1.0 are represented by black, blue and orange solid lines, respectively. Insets show magnification of the loops at lower fields.

Table 2. Parameters estimated from the hysteresis curves.

	M_s (emu g^{-1})			H_c (Oe)			M_r (emu g^{-1})		
x	C	HT	FH	C	HT	FH	C	HT	FH
0.0	60.93	70.52	32.00	1805.15	970.41	2.18	39.08	17.08	0.02
0.4	40.47	59.28	38.40	934.27	1376.43	1.42	13.21	22.36	0.02
1.0	40.10	48.03	21.78	179.30	15.09	1.72	10.33	9.09	0.01

Differently from the saturation magnetization (M_s), herein found to be mainly dependent on the grain size and cation distribution, the coercive field (H_c) has proved to be highly sensitive to the stoichiometry. Data collected in table 2 and in the insets of figures 2(a) and (c) show that cobalt-rich samples synthesized via both C-and FH-method present higher H_c values. This finding can be explained by the obtained crystalline anisotropy values ($K_{CoFe2O4} > K_{NiFe2O4}$); the larger the crystalline anisotropy (K), which is the case of cobalt-rich samples, the higher the field ($H = H_c$) required to revert the previously aligned spins [26, 29]. Once more, the samples synthesized via the HT-method show the opposite trend for $x = 0.0$ and 0.4 (see data in table 2), revealing larger H_c value (1376 Oe) for lower cobalt content ($x = 0.4$). In this particular case (HT-method), it is interesting to analyze the combined effect of crystalline anisotropy and grain size for two samples ($x = 0.0$ and 0.4). Here, the smaller grain size (16 nm), occurring for the cobalt-richest sample ($x = 0.0$), presents lower coercive field (970 Oe); this effect is well known and can be described through the following expression [26]:

$$H_c = A_K(1 - D_P/D)^{2/3}, \tag{3}$$

where, for a specific spherical nanoparticle, D_P is the critical diameter above which the magnetocrystalline energy (KV) acquires relevant values relatively to the thermal energy (KT). A_K is just a constant while de sub-index (K) is used to pointing out the overlapped dependence with the magnetocrystaline anisotropy, i.e., $A_K \propto H_K$. We claim that the grain size effect overlaps with the anisotropy effect; the smaller grain size (16 nm) drives the system towards superparamagnetic behavior, thus reducing the coercive field. Even for the fraction of the $x = 0.0$ sample outside the superparamagnetic regime, the applied magnetic field required to overcome the magnetocrystalline energy barrier is facilitated due tothe proximity of the superparamagnetic regime. This understanding also agrees well with the model proposed in the literature [30]. On the other hand, the HT-sample, with $x = 1.0$ (diameter $D \approx 80$ nm), has a very small H_c ($\approx$15 Oe), suggesting the occurrence of magnetic multi-domains ($D > D_c \equiv$ maximum diameter of magnetic monodomain) and, consequently, leading to the decrease of Hc. This effect is also well known and is experimentally found to be given approximately by [26]:

$$H_c = a + \frac{b}{D}, \tag{4}$$

where a and b are constants. The limiting region of action for equations (3) and (4) defines the region of maximum value for H_c.

Room-temperature ferromagnetic resonance (FMR) of all prepared samples ($Co_{1-x}Ni_xFe_2O_4$; $x = 0.0$, 0.4, and 1.0), fabricated using the three synthetic routes (C, FH, and HT), are shown in figure 3. Solid lines in figure 3 represent experimental data whereas spectra simulations are represented by dotted lines, being the parameters extracted from the FMR spectra simulations collected in table 3. All FMR spectra show large peak-to-peak width

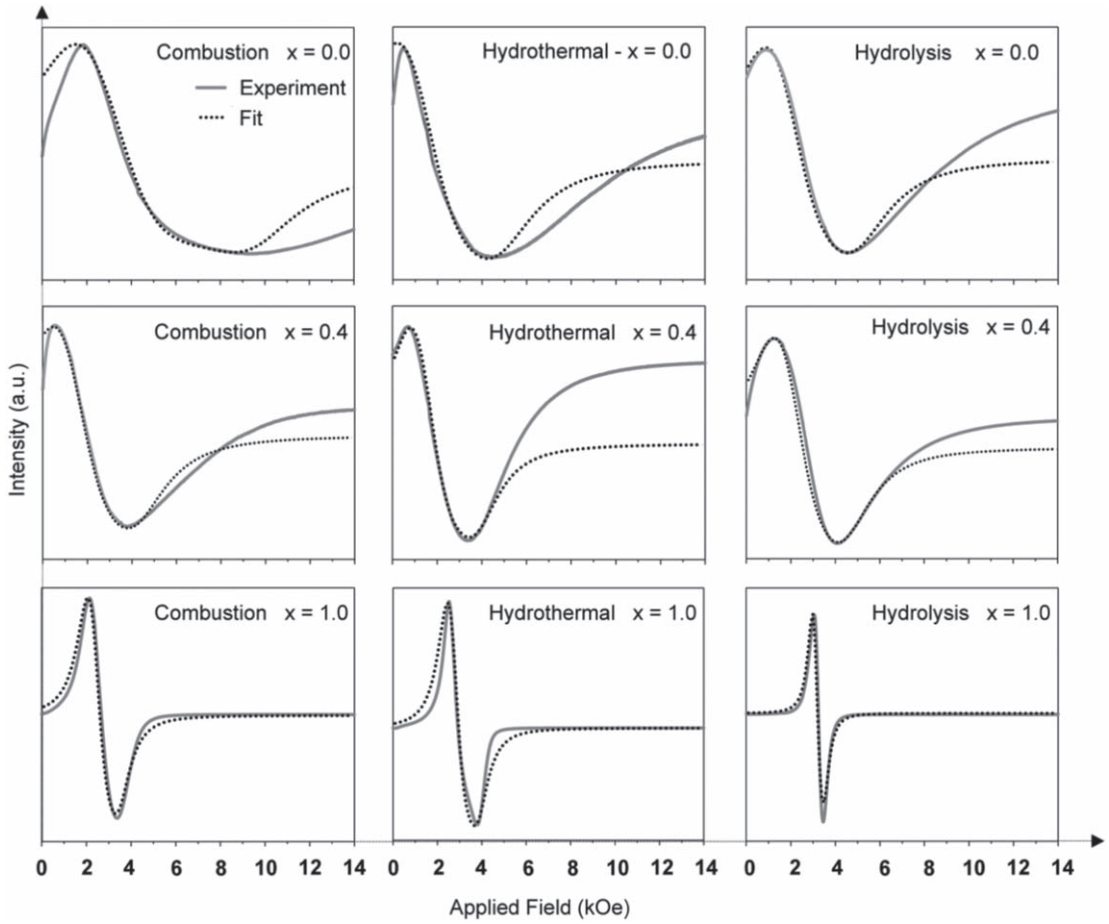

Figure 3. FMR spectra (solid lines) and spectra simulation (dashed lines) for the samples obtained using the combustion, hydrothermal treatment and forced hydrolysis methods ($x = 0.0, 0.4$, and 1.0).

Table 3. Parameters obtained from de FMR spectra simulations.

	W(Oe)			H_a(Oe)			g-factor			ΔH_{pp}(Oe)		
x	C	HT	FH	C	HT	FH	C	HT	FH	C	HT	FH
0.0	1600	1300	1200	−4600	−2445	−2165	1.50	3.25	2.65	7660	4075	3610
0.4	1100	800	980	−1968	−1620	−1660	3.35	3.40	2.65	3280	2700	2765
1.0	400	350	180	−747	−769	−252	2.62	2.32	2.19	1245	1282	420

(ΔH_{pp}) and high spectrum dispersion parameter (W) [31]. Except for the$NiFe_2O_4$ ($x = 1$) sample, obtained by the FH-method, the large asymmetry observed in all FMR spectra are quite similar and successfully explained usingthe model picture of randomly orientation of thecore crystalline structure [32]. The unusual behavior of the $NiFe_2O_4$ sample, synthesized via the FH-method, showing very much symmetric FMR spectrum, can be accounted for by the observed reduced grain size(5.5 nm), with large surface-to-volume ratio, thus minimizing the impact of the core crystalline component on the spectrum asymmetry. Data collected in table 3 and spectra shown in figure 3 reveal the trend of increasing FMR spectrum symmetry as the average grain size is reduced.

An inverse behavior is observed for the samples obtained by the HT-method. In this case, the highest FMR line symmetry occurs for the largest grain size (about 80 nm). We infer that the mechanism behind this behavior is the onset of magnetic multidomain. As the particlesize increases, each domain comes under aleatory influence of randomly arranged neighboring domains. This random dipolar magnetic interaction overlaps the crystalline anisotropy field, resulting in apparent reduced anisotropy and, consequently, in more symmetric FMR line shape. This hypothesis leads to two further conclusions: (a) the model proposed by Tsay*et al* [23] may be applied for magnetic nanoparticles with non-interacting monodomains; (b) the effect of the onset magnetic multidomain can be signaled by both decreasing of the coercivity and increasing symmetry of the FMR line

shape. However, a more systematic study with systems of the same stoichiometry should be performed to confirm this hypothesis.

It is worth noticing in table 3 the decrease of the peak-to-peak width (ΔH_{pp}) while the nickel-content (x) increases. This trend is in agreement with smaller absolute value of the crystalline anisotropy for nickel ferrites ($x = 1$) relative to cobalt ferrites ($x = 0$), represented by the extracted values of the magnetocrystalline anisotropy field (see data in table 3). Indeed, the highest the value of the magnetocrystalline anisotropy field the strongest the external magnetic field variation capable of sweeping the entire range of anisotropy—from the {111} direction towards the {100} direction, representing the larger (positive) and the smaller (negative) crystalline anisotropy, respectively [24].

Table 3 also collects the g-factor ($g = \frac{h\nu}{\beta H_{eff}}$), where h is the Planck's constant, ν is the microwave frequency, β is the Bohr's magneton and H_{eff} is the effective magnetic field acting on the sample. The model proposed by Tsay *et al* for FMR spectra simulations includes only the magnetocrystalline anisotropy field [23]. This means that other contributions to the field, such as dipolar, demagnetizing (shape anisotropy) and stress are incorporated into the g-factor, once g is used as a fitting parameter. Thus, the g-factor is the only parameter responsible for displacing the simulated spectra horizontally, reflecting some unusual g-values.

4. Conclusions

In summary, three sets of $Co_{1-x}Ni_xFe_2O_4$ ($x = 0.0$, 0.4, and 1.0) nanoparticles (NPs) are successfully fabricated using three different synthetic routes, namely combustion (C), hydrothermal (HT), and forced hydrolysis (FH). X-ray diffraction (XRD) confirmed the face centered cubic (fcc) spinel structure of all synthesized samples and estimated the average grain size (D). Hysteresis cycles (HC) and ferromagnetic resonance (FMR) are used to assess the saturation magnetization (M_s), coercive field (H_c), remanence (M_r), and magnetocrystalline anisotropy field (H_a). The results obtained from the FMR are in very good agreement with those obtained from the XRD data, indicating cubic structures. From the FMR fittings herein introduced, it is possible to obtain the crystalline anisotropy fields—in the $\langle 111 \rangle$ direction (negative anisotropy)—and to associate the evolution for the anisotropywith the synthesis route. By varying the stoichiometry (x) in the range of $0.0 \leqslant x \leqslant 1.0$ the C- and HT-method successfully fabricated $Co_{1-x}Ni_xFe_2O_4$ NPs with$15\ \text{nm} < D < 80\ \text{nm}$whereas the FH-method provided $Co_{1-x}Ni_xFe_2O_4$ NPs with $5\ \text{nm} < D < 10\ \text{nm}$. As a result of modulating the average grain size in the range of $5\ \text{nm} < D < 80\ \text{nm}$we succeeded in modulating the saturation magnetization ($20\ \text{emu g}^{-1} < M_s < 70\ \text{emu g}^{-1}$), coercive field ($1\ \text{Oe} < H_c < 1800\ \text{Oe}$), remanence ($0.01\ \text{emu g}^{-1} < M_r < 30\ \text{emu g}^{-1}$), and magnetocrystalline anisotropy field ($-4600\ \text{Oe} < H_a < -250\ \text{Oe}$). Moreover, we found M_s primarily depending upon D whereas H_c mostly depends upon x. We also suggest a qualitative model that links the increasingFMR spectra symmetry–decreasing anisotropy H_a–with the emergence of magnetic multidomain; establishing a validity limit for obtaining magnetocrystalline anisotropies through the theoretical fitting proposed by Tsay *et al* [23].

Indeed, the structural and magnetic data herein reported strongly support the use of a multi-synthetic route platform for fabrication of nanosized mixed cubic ferrites, aiming to modulate key magnetic properties in a wide range of values in order to meet different requirements of technological applications.

Acknowledgments

We acknowledge the support provided by the Conselho Nacional de DesenvolvimentoCientífico e Tecnológico -CNPq, Brazil (Grant Ns. 435229/2018-4 and 310440/2018-1).

ORCID iDs

M S Pessoa https://orcid.org/0000-0001-6117-8492

References

[1] Dionne G F 2009 Magnetic ions in oxides *Magn. Oxides* (US, Boston, MA: Springer) pp 37–106
[2] Szotek Z, Temmerman W M, Koedderitzsch D, Svane A, Petit L and Winter H 2006 *Electronic Structure of Normal and Inverse Spinel Ferrites from First Principles* **74** 174431
[3] Manjurul Haque M, Huq M and Hakim M A 2009 Effect of Zn^{2+} substitution on the magnetic properties of $Mg_{1-x}Zn_xFe_2O_4$ ferrites *Phys. B Condens. Matter.* **404** 3915–21
[4] Zhao L J and Jiang Q 2010 Effects of applied magnetic field and pressures on the magnetic properties of nanocrystalline $CoFe_2O_4$ ferrite *J. Magn. Magn. Mater.* **322** 2485–7

[5] Zhong J, Liu W, Kong L and Morais P C 2015 A new approach for highly accurate, remote temperature probing using magnetic nanoparticles *Sci. Rep.* **4** 6338

[6] Nguyen T, Kremer L N, Longtin D J, Lehmann M N, Duggan G G, Wagner L, Cornelius S C, Stark J L and Price X M 2011 *Method of Removing Multi-Valent Metals from Crude Oil* https://patents.google.com/patent/EP2601277A2/en

[7] Amirabadizadeh A, Salighe Z, Sarhaddi R and Lotfollahi Z 2017 Synthesis of ferrofluids based on cobalt ferrite nanoparticles: influence of reaction time on structural, morphological and magnetic properties *J. Magn. Magn. Mater.* **434** 78–85

[8] Gholizadeh A 2019 The effects of A/B-site substitution on structural, redox and catalytic properties of lanthanum ferrite nanoparticles *J. Mater. Res. Technol.* **8** 457–66

[9] Daffé N, Gavrilov V, Neveu S, Choueikani F, Arrio M A, Juhin A, Ohresser P, Dupuis V and Sainctavit P 2019 Small $CoFe_2O_4$ magnetic nanoparticles in ferrofluids, influence of the synthesis on the magnetic anisotropies *J. Magn. Magn. Mater.* **477** 226–31

[10] Pourgolmohammad B, Masoudpanah S M and Aboutalebi M R 2017 Synthesis of $CoFe_2O_4$ powders with high surface area by solution combustion method: effect of fuel content and cobalt precursor *Ceram. Int.* **43** 3797–803

[11] Gholizadeh A and Jafari E 2017 Effects of sintering atmosphere and temperature on structural and magnetic properties of Ni–Cu–Zn ferrite nano-particles: magnetic enhancement by a reducing atmosphere *J. Magn. Magn. Mater.* **422** 328–36

[12] Gholizadeh A 2018 A comparative study of the physical properties of Cu–Zn ferrites annealed under different atmospheres and temperatures: magnetic enhancement of $Cu_{0.5}Zn_{0.5}Fe_2O_4$ nanoparticles by a reducing atmosphere *J. Magn. Magn. Mater.* **452** 389–97

[13] Ben Osman C, Barthas E, Decorse P and Mammeri F 2019 Surface functionalization of $CoFe_2O_4$ nanoparticles for driving the crystallization of the electroactive β-PVDF through judicious tailoring of the hybrid interface *Colloids Surfaces A Physicochem. Eng. Asp.* **577** 405–11

[14] Mantilla J *et al* 2018 Washing effect on the structural and magnetic properties of $NiFe_2O_4$ nanoparticles synthesized by chemical sol-gel method *Mater. Chem. Phys.* **213** 295–304

[15] Franco A, Machado F L A, Zapf V S and Wolff-Fabris F 2011 Enhanced magnetic properties of Bi-substituted cobalt ferrites *J. Appl. Phys.* **109** 07A745

[16] Franco A, Silva F C E and Zapf V S 2012 High temperature magnetic properties of $Co_{1-x}Mg_xFe_2O_4$ nanoparticles prepared by forced hydrolysis method *J. Appl. Phys.* **111** 07B530

[17] Melo R S, Banerjee P and Franco A 2018 Hydrothermal synthesis of nickel doped cobalt ferrite nanoparticles: optical and magnetic properties *J. Mater. Sci., Mater. Electron.* **29** 14657–67

[18] Caetano P M A, Albuquerque A S, Fernandez-Outon L E, Macedo W A A and Ardisson J D 2018 Structure, magnetism and magnetic induction heating of $Ni_xCo_{(1-x)}Fe_2O_4$ nanoparticles *J. Alloys Compd.* **758** 247–55

[19] Houshiar M, Zebhi F, Razi Z J, Alidoust A and Askari Z 2014 Synthesis of cobalt ferrite ($CoFe_2O_4$) nanoparticles using combustion, coprecipitation, and precipitation methods: a comparison study of size, structural, and magnetic properties *J. Magn. Magn. Mater.* **371** 43–8

[20] Datt G, Sen Bishwas M, Manivel Raja M and Abhyankar A C 2016 Observation of magnetic anomalies in one-step solvothermally synthesized nickel–cobalt ferrite nanoparticles *Nanoscale.* **8** 5200–13

[21] Gholizadeh A 2017 A comparative study of physical properties in Fe_3O_4 nanoparticles prepared by coprecipitation and citrate methods *J. Am. Ceram. Soc.* **100** 3577–88

[22] Shamgani N and Gholizadeh A 2019 Structural, magnetic and elastic properties of $Mn_{0.3-x}Mg_xCu_{0.2}Zn_{0.5}Fe_3O_4$ nanoparticles *Ceram. Int.* **45** 239–46

[23] Tsay F-D, Chan S I and Manatt S L 1971 Ferromagnetic resonance of lunar samples *Geochim. Cosmochim. Acta* **35** 865–75

[24] Pessoa M S, Proveti J R C, Pelegrini F and Moscon P S 2019 Ferromagnetic resonance lines of annealed Ni ferrites *Phys. B Condens. Matter.* **558** 20–3

[25] Morais P C, Lara M C L and Neto K S 1987 Electron spin resonance in superparamagnetic particles dispersed in a non-magnetic matrix *Philos. Mag. Lett.* **55** 181–3

[26] Cullity B D and Graham C D 2011 *Introduction to Magnetic Materials* (New York: Wiley) https://books.google.com.br/books/about/Introduction_to_Magnetic_Materials.html?id=fh_F0G9KuSgC&redir_esc=y

[27] Chikazumi S and Graham C D 2009 *Physics of Ferromagnetism 2e* (Oxford: OUP) https://books.google.com/books?id=f8pdPk3RuowC&pgis=1

[28] Li Y, Li Q, Wen M, Zhang Y, Zhai Y, Xie Z, Xu F and Wei S 2007 Magnetic properties and local structure studies of Zn doped ferrites *J. Electron Spectros. Relat. Phenomena.* **160** 1–6

[29] Fayling R E 1978 Relationship between coercive force and anisotropy field for oriented barium ferrite tapes and magnets *J. Appl. Phys.* **49** 1823–5

[30] Kneller E F and Luborsky F E 1963 Particle size dependence of coercivity and remanence of single-domain particles *J. Appl. Phys.* **34** 656–8

[31] Sukhov A, Usadel K D and Nowak U 2008 Ferromagnetic resonance in an ensemble of nanoparticles with randomly distributed anisotropy axes *J. Magn. Magn. Mater.* **320** 31–5

[32] Griscom D L 1984 Ferromagnetic resonance of precipitated phases in natural glasses *J. Non. Cryst. Solids.* **67** 81–118